Featured in Physics

Signatures of Ultralight Bosons in the Orbital Eccentricity of Binary Black Holes

Mateja Bošković,[1,*] Matthias Koschnitzke,[1,2,†] and Rafael A. Porto[1,‡]
[1]Deutsches Elektronen-Synchrotron DESY, Notkestraße 85, 22607 Hamburg, Germany
[2]II. Institut für Theoretische Physik, Universität Hamburg, Luruper Chaussee 149, 22761 Hamburg, Germany

(Received 14 March 2024; accepted 14 August 2024; published 16 September 2024)

We show that the existence of clouds of ultralight particles surrounding black holes during their cosmological history as members of a binary system can leave a measurable imprint on the distribution of masses and orbital eccentricities observable with future gravitational-wave detectors. Notably, we find that for nonprecessing binaries with chirp masses $\mathcal{M} \lesssim 10M_\odot$, formed exclusively in isolation, larger-than-expected values of the eccentricity, i.e., $e \gtrsim 10^{-2}$ at gravitational-wave frequencies $f_{\rm GW} \simeq 10^{-2}$ Hz, would provide tantalizing evidence for a new particle of mass between $[0.5, 2.5] \times 10^{-12}$ eV in nature. The predicted evolution of the eccentricity can also drastically affect the in-band phase evolution and peak frequency. These results constitute unique signatures of boson clouds of ultralight particles in the dynamics of binary black holes, which will be readily accessible with the Laser Interferometer Space Antenna, as well as future midband and decihertz detectors.

DOI: 10.1103/PhysRevLett.133.121401

Introduction—The birth of gravitational-wave (GW) science [1] heralds a new era of discoveries in astrophysics, cosmology, and particle physics [2]. Measuring the properties of GW signals with current and future observatories, such as the Laser Interferometer Space Antenna (LISA) [3], the Einstein Telescope (ET) [4], and Cosmic Explorer (CE) [5], as well as other midband [6] and decihertz detectors [7], not only will unravel the origins of binary black hole (BBH) mergers, it also opens the possibility to discover (very-weakly-coupled) ultralight particles that are ubiquitous in theories of the early Universe [8–12]. Notably, the mass, spin alignment, and eccentricity are expected to be correlated with formation channels, *isolated* or *dynamical*, e.g., [13–31]; whereas boson clouds (or "gravitational atoms" [8,9]), formed around black holes via superradiance instabilities [32–36], can produce a large backreaction on the orbital evolution. Following analogies with atomic physics [37], the cloud may encounter Landau-Zener (LZ) resonances [38], or ionization effects [39–41]. The presence of a cloud then leads to large finite-size effects [37,42], floating and sinking orbits [38], as well as other sharp features [40], that become unique signatures of ultralight particles in the BBH dynamics.

For the most part, up until now, backreaction effects have been studied under the simplified assumption of planar, quasicircular orbits. The reason is twofold [37]. First, several formation scenarios lead to spins that are parallel to the orbital angular momentum [18]. Second, the decay of eccentricity through GW emission in vacuum [43,44] is expected to have circularized the orbit in the late stages of the BBH dynamics. We retain here the former but relax the latter assumption. As we shall see, adding eccentricity not only introduces a series of *overtones* [41,45,46], it can also have a dramatic influence in the orbital dynamics as the cloud transits a LZ-type transition. Although the strength of the new resonances is proportional to the eccentricity, depending on their position and nature (floating or sinking), a small departure from circularity can lead to transitions that not only would deplete the cloud, but also induce a rapid growth of eccentricity toward a large critical (fixed-point) value: $e_{\rm cr} \in [0.3, 0.6]$. As measurements of the eccentricity are correlated with formation channels, the predicted increase can impact the inferred binary's origins. Measurements of larger-than-expected eccentricities would then provide strong evidence for the existence of a new ultralight particle in nature. In particular, because of the critical fixed point, a fraction of the BBHs undergo a rapid growth of orbital eccentricity to a common value. As a result, the distribution of masses and eccentricities may feature a skewed correlation by the time they reach the detector's band. Furthermore, for chirp masses $\mathcal{M} < 10M_\odot$ and spin(s) aligned with the orbital angular momentum—expected to exclusively form in the field—the presence of a boson cloud at earlier times can shift a fraction of the population toward values of $e \gtrsim 10^{-2}$ at 10^{-2} Hz, readily accessible to LISA [3]. Furthermore, the GW-evolved eccentricity may also be within reach of the planned midband [6] or decihertz [7] observatories. For all such events, a new ultralight boson of mass $[0.5, 2.5] \times 10^{-12}$ eV forming a cloud and decaying through a LZ-type transition prior to detection, may be the ultimate culprit.

The more drastic evidence is given when the resonant transition occurs in band with measurable frequency evolution. A plethora of phenomena are discussed in

*Contact author: mateja.boskovic@desy.de
†Contact author: matthias.koschnitzke@desy.de
‡Contact author: rafael.porto@desy.de

[37,38] for circular orbits. In addition to overtones, the increase in eccentricity would imply that higher harmonics become more relevant, which in turn affects the peak frequency of the GWs, even for floating orbits. We point out here some salient features and elaborate further on the details elsewhere [46].

The gravitational atom—Ultralight particles of mass μ can form a cloud around a rotating black hole of mass M, via superradiant instabilities [8,9]. The typical mass of the (initial) cloud scales as $M_{c,0}/M \simeq \alpha$, whereas its typical size is $r_c \simeq (r_g/\alpha^2)$, with $r_g \equiv (GM/c^2)$, and

$$\alpha = \frac{GM\mu}{\hbar c} \simeq 0.1\left(\frac{M}{15M_\odot}\right)\left(\frac{\mu}{10^{-12}\ \mathrm{eV}}\right). \tag{1}$$

The (scalar) cloud evolves according to a Schrödinger-like equation [47,48], with eigenstates $|a\rangle \equiv |n_a l_a m_a\rangle$, and (n, l, m) the principal, orbital, and azimuthal angular momentum, "quantum numbers." (For vector clouds [38,48,49], we must include the total angular momentum.)

The energy eigenvalues of the cloud scale as $\epsilon_{nlm} = \mu\left[1 - (\alpha^2/2n^2) + f_{nl}\alpha^4 + h_{nl}\tilde{a}m\alpha^5\right]$, with $\tilde{a}$ the dimensionless spin of the black hole, see Ref. [48]. At saturation, we have $\tilde{a} \simeq \alpha$, whereas the combined system black hole plus cloud may still be rapidly rotating. One of the main difference with respect to ordinary atoms, however, is the presence of a decay or growing time, $\Gamma_{nlm}^{-1} \propto \mu\alpha^{4l+5}$, for a given eigenstate [9,47,48,50]. The (scalar) cloud may be populated by the dominant *growing* mode, $|211\rangle$, or an *excited* state, $|322\rangle$. Depending on α, they may be robust to GW emission (from the cloud itself) on astrophysical scales [9,51–55]. They can also deplete through resonant transitions in binaries [37,38], as we discuss here. In what follows we work with $G = \hbar = c = 1$ units.

Gravitational collider goes eccentric—Following [37,38] we consider a boson cloud around a black hole of mass M in a bound orbit with a companion object of mass $M_\star$, with $q \equiv M_\star/M$ the mass ratio. The coordinates are centered at the black hole plus cloud system, with $R_\star$ the radial distance to the perturber, and $\varphi_\star$ the azimuthal angle. We consider planar motion with the spin parallel to the orbital angular momentum, with the orbit described by the semimajor axis a and the eccentricity e, while $\varphi_\star$ corresponds to the true anomaly. We take the orbital frequency to be positive such that the two, corotating and the counterrotating, orientations are identified by $\dot{\varphi}_\star = s|\dot{\varphi}_\star|$, with $s = \pm 1$.

The gravitational perturbations of the companion induce mixing of the atomic levels. For a perturber outside of the cloud $R_\star \gg r_c$ the off-diagonal matrix elements of the Hamiltonian, $\langle a|V_\star|b\rangle$, are given by a multipole expansion that can be written as an harmonic series [37,38]

$$\langle a|V_\star|b\rangle_{l_\star} = \sum_{|m_\star|\leq l_\star} \eta_{ab}^{(m_\star)} e^{-im_\star\varphi_\star}, \tag{2}$$

with $\eta_{ab}^{(m_\star)} \propto R_\star^{-(l_\star+1)}$. The matrix elements obey selection rules which determine possible transitions, which we refer as hyperfine (only $\Delta m \neq 0$), fine $(\Delta\ell \neq 0, \Delta n = 0)$, and Bohr $(\Delta n \neq 0)$, respectively [37,38].

For illustrative purposes, we consider a two-level model. The Hamiltonian equation is given by

$$i\begin{pmatrix}\dot{c}_a\\ \dot{c}_b\end{pmatrix} = \begin{pmatrix}-\frac{\Delta\epsilon}{2} & \eta_0\left(\frac{R_\star}{R_0}\right)^{-(l_\star+1)}e^{i\Delta m\varphi_\star}\\ \text{c.c.} & \frac{\Delta\epsilon}{2} - i\Gamma_b\end{pmatrix}\begin{pmatrix}c_a\\ c_b\end{pmatrix}, \tag{3}$$

with $\Delta m \equiv m_b - m_a$, $\Delta\epsilon \equiv \epsilon_b - \epsilon_a$ the energy split, Γ_b the width of the decaying mode, and η_0 the value of the perturbation at a reference point R_0. Furthermore, since (vacuum) GW emission is expected to reduce the initial eccentricity prior to encountering the resonant transition, and for the purpose of analytical understanding, in what follows we describe the orbital evolution in the Hamiltonian $\mathcal{H}$ of (3) using a small-eccentricity approximation [56],

$$\varphi_\star \simeq \vartheta + 2e\sin\vartheta, \qquad R_\star \simeq a(1 - e\cos\vartheta), \tag{4}$$

$$\dot{\vartheta} \equiv s\Omega, \qquad \Omega = \sqrt{M(1+q)/a^3}, \tag{5}$$

in terms of ϑ, the mean anomaly [72], and apply the Jacobi-Anger expansion into Bessel functions. Hence,

$$\mathcal{H} = \mathcal{D} + \sum_{k=-\infty}^{\infty}\begin{pmatrix}0 & \eta_k e^{i(k+\Delta m)\vartheta}\\ \eta_k e^{-i(k+\Delta m)\vartheta} & 0\end{pmatrix},$$
$$\mathcal{D} = \begin{pmatrix}-\frac{\Delta\epsilon}{2} & 0\\ 0 & \frac{\Delta\epsilon}{2} - i\Gamma_b\end{pmatrix}, \quad \eta_k \sim \eta_0 \mathfrak{f}^{\frac{2}{3}(l_\star+1)}\frac{e^{|k|}}{|k|!}, \quad \mathfrak{f} \equiv \frac{\Omega}{\Omega_0}, \tag{6}$$

where we traded distance for orbital frequency. The case $(e, \Gamma_b) = 0$ was studied in [38]. The slow GW-induced evolution of the orbital frequency, $\Omega(t) \simeq \Omega_0 + \gamma_0 t$ with $\gamma_0 = (96/5)qM^{5/3}[\Omega_0^{11/3}/(1+q)^{1/3}]$, leads to a LZ transition [73,74] between the energy levels. The transition is triggered for

$$\Omega_0 = s\frac{\Delta\epsilon}{\Delta m} > 0. \tag{7}$$

This value, dictated by the spectrum of the cloud, will serve as our reference point in the evolution of the binary.

Ignoring backreaction effects (see below), the LZ solution is controlled by the parameter $z_0 \equiv \eta_0^2/(\gamma_0|\Delta m|)$, which determines the adiabaticity of the transition. As famously demonstrated in [73,74], starting in the far past from the $|a\rangle$ state, in the limit $2\pi z_0 \gg 1$, the eigenstate of the (time-dependent) Hamiltonian yields a complete population transfer into the (decaying) $|b\rangle$ mode in the far future. As it turns out, although the solution changes at finite time, controlled by the parameter $v_0 \equiv \Gamma_b/\sqrt{\gamma_0|\Delta m|}$, the asymptotic properties of the system (ignoring backreaction) are remarkably robust against the value of the decaying width for the $|b\rangle$ state [75].

For eccentric orbits, the evolution in (6) also features a transition at Ω_0 (for $k = 0$). However, it introduces a series

of overtones

$$\Omega_k = \mathfrak{f}_k \Omega_0, \qquad \mathfrak{f}_k = \frac{\Delta m}{\Delta m + k}, \qquad k \in \mathbb{Z}. \tag{8}$$

Provided each k resonance is sufficiently narrow, we can ignore the other ($k' \neq k$) terms in (6). As in [38], we can linearize the orbital evolution near the transition, $\Omega(t) = \Omega_k + f(e)\gamma_k t$, where $f(e) = \{[1 + (73e^2/24) + (37e^4/96)]/(1-e^2)^{7/2}\}$ and $\gamma_k \equiv \gamma_0 \mathfrak{f}_k^{11/3}$, such that the LZ solution now depends on the modified $z_k \equiv \eta_k^2/[f(e)\gamma_k|\Delta m + k|]$ and $v_k \equiv (\Gamma_b/\sqrt{f(e)\gamma_k|\Delta m + k|})$, respectively.

Orbital backreaction—Dissipative effects, such as GW emission, from the binary [38,76] or the cloud itself [51–55], ionization [39–41,76], and decay widths [75,77,78], strongly influence the LZ phenomenology, and vice versa. We focus here on the prevailing case of two-body GW emission, with the companion *outside* of the cloud, thus focusing on (hyper)fine resonances, combined with a two-level LZ transition into a decaying mode.

The orbital dynamics is governed by flux-balance equations at infinity [38,41,44,46,78,79], and at the black hole's horizon [8,80,81]:

$$\dot{E}_{\rm o} + \dot{E}_{\rm c} + \dot{M} = \mathcal{F}_{\rm GW} \equiv -\frac{32 f(e)}{5}\frac{M^5 q^2 (q+1)}{a^5}, \tag{9}$$

$$\dot{L}_{\rm o} + s(\dot{L}_{\rm c} + \dot{S}) = \mathcal{T}_{\rm GW} \equiv \frac{\mathcal{F}_{\rm GW}}{\Omega}\frac{g(e)}{f(e)}, \tag{10}$$

$$\dot{M} = 2\Gamma_b E_{{\rm c}(b)}, \qquad \dot{S} = 2\Gamma_b L_{{\rm c}(b)}, \tag{11}$$

with $g(e) = \{[1 + (7e^2/8)]/(1-e^2)^2\}$, and $\dot{M}$, $\dot{S}$ the change of mass and spin due to the decay of the $|b\rangle$ state onto the black hole [82].

The orbital energy and angular momentum are given by $E_{\rm o} = -(M^2 q/2a)$ and $L_0^2 = (M^5 q^3)(1-e^2)/[2(q+1)|E_{\rm o}|]$, while for the cloud is a sum over the populated states, $E_{{\rm c}(i)} \equiv (M_{\rm c,0}/\mu)\epsilon_i |c_i|^2$, and similarly for $L_{{\rm c}(i)}$ with $\epsilon_i \to m_i$.

The above equations can then be rewritten as

$$\frac{d\Omega}{dt} = r\gamma_0 \mathfrak{f}^{11/3} f(e), \tag{12}$$

$$r \equiv \frac{\dot{E}_{\rm o}}{\mathcal{F}_{\rm GW}} = 1 - b\,\frac{{\rm sgn}(s\Delta m)\mathfrak{f}^{-11/6}}{\sqrt{f(e)\gamma_0|\Delta m + k|}}\frac{d|c_a|^2}{dt}, \tag{13}$$

$$\frac{de^2}{dt} = \frac{2}{3}\mathfrak{f}^{8/3}\frac{\gamma_0}{\Omega_0} f(e)\sqrt{1-e^2} \times \left[r\left(\mathfrak{f} - \sqrt{1-e^2}\right) - \mathfrak{f} + \frac{g(e)}{f(e)}\right], \tag{14}$$

in terms of the orbital parameters, where

$$b \equiv \frac{3M_{\rm c,0}}{M}\frac{|\Delta m|\mathfrak{f}^{-3/2}}{|\Delta m + k|^{-1/2}}\frac{(1+q)^{1/3}}{\alpha q}\frac{(M\Omega_0)^{1/3}\Omega_0}{\sqrt{\gamma_0}}, \tag{15}$$

parametrizes the backreaction effects on the orbit due to the cloud. It is worth emphasising that the above equations apply to generic (planar) motion, regardless of the value for the eccentricity. As we shall see, even for small initial conditions, the orbit is affected by large backreaction effects due to the presence of the cloud.

As anticipated by the analysis in [38] for the case of circular orbits (which we encourage the reader to consult for further details), "effective" LZ parameters emerge: $\zeta_k(t) \equiv z_k/r(t)$ and $w_k(t) \equiv v_k/\sqrt{r(t)}$, making it a fully nonlinear system. We can nonetheless estimate the value of the energy-momentum transfer near the resonance by self-consistently solving the condition $\zeta_k = z_k/r_k(\zeta_k)$. For moderate-to-large population transfer ($\zeta_k \gtrsim 1$), we find the limiting results:

$$r_k \simeq \left(1 - {\rm sgn}(s\Delta m)\frac{b_k}{4\sqrt{z_k}}\right)^{-1}, \quad (w_k \ll \zeta_k)$$

$$r_k \simeq 2\left(1 + \sqrt{1 - {\rm sgn}(s\Delta m)\frac{b_k}{z_k v_k}}\right)^{-1}, \quad (w_k \gg \zeta_k). \tag{16}$$

As discussed in [38], the orbital evolution branches into either floating ($r \simeq 0$), for $s\Delta m < 0$, or sinking orbits ($r \gtrsim 1$), for $s\Delta m > 0$. However, except for the trivial case when $\zeta_k \ll 1$, due to the nonlinear nature of the problem the transfer of energy and angular momentum from the cloud to the orbit does not simply reduce to the quest for adiabaticity of the LZ transition, not even for $w_k \ll \zeta_k$. For instance, for extreme cases, with $z_k \gg 1$, the (unperturbed) transition spreads over long timescales, $\Delta t_{\rm LZ} \simeq 4\sqrt{z_k/\gamma_k}$ [83], which in turn reduces the orbital impact, as we see in (16). As it turns out, in the large backreaction scenario, the sweet spot for floating orbits occurs when $b_k \gg \sqrt{z_k}$. Even though, due to the properties of the LZ solution, a strong decay width ($w_k \gg \zeta_k$) does not alter this picture, the impact on the orbit evolution as well as the population transfer becomes suppressed by $1/v_k$, as shown in (16). On the other hand, for the sinking case, the largest values of r_k are obtained for nonadiabatic transitions.

Eccentric fixed point—For the GW-dominated epochs, with $r \simeq 1$, the leading order term in (14) vanishes, and the first contribution is at $\mathcal{O}(e^2)$. Likewise, for the $k = 0$ (main) resonance, for which the first term is $\propto \left[(r/2) - (11/3)\right]e^2$. As a result, the eccentricity is damped unless the orbit gets a large kick ($r \gtrsim 7.3$). As the influence of the cloud increases, the rhs of (14) asymptotes (modulo a positive prefactor) to $(\mathfrak{f}_k - 1)(r-1)$, in which case it enters at leading order. Moreover, the differences in the GW fluxes in (9) and (10)

generate a distinction between the early and late resonances. In the floating case, with $r \simeq 0$, the eccentricity grows for the early resonances ($\mathfrak{f}_k < 1$) and decays for the late ones ($\mathfrak{f}_k > 1$). This can be understood by noticing that, when $\dot{E}_o \simeq 0$, we have $\dot{L}_0 \propto [(\Omega - \Omega_0)/(\Omega\Omega_0) + \mathcal{O}(e^2)]$ and using $d(L_o^2) \propto -d(e^2)$ the eccentricity grows for $\Omega_k < \Omega_0$ and decays whenever $\Omega_k \geq \Omega_0$. This trend is reversed in the sinking case.

Because of the changes in the evolution of the eccentricity across different resonances, it is instructive to look at the opposite limit $e \to 1$. In that case, the rhs of (14) becomes $\propto [(r-1)/(1-e)^3]$. Let us consider the case of a floating orbit. Since the sign of (de/dt) is positive for $\Omega_k < \Omega_0$, but turns negative when the eccentricity approaches $e \simeq 1$, this implies the existence of a critical "attractor" fixed point, $e_{\rm cr}$, given by the condition $g(e_{\rm cr})/f(e_{cr}) = \mathfrak{f}_k$ [cf. (14)]. For instance,

$$e_{\rm cr} = \{0.46, 0.35, 0.29\}, \quad \text{for } |\Delta m| = \{1, 2, 3\}, \quad (17)$$

with $k = -1$. Similarly, an unstable fixed point develops for the earlier and main sinking resonances.

For the case of floating orbits (with $s\Delta m < 0$), if the backreaction is sufficiently effective to enforce $r_k \simeq 0$ while the eccentricity approaches the critical point, one can then estimate the floating time $\Delta t_{\rm FL} \simeq b_k/\sqrt{\gamma_k}$, leftover population $|c_a(\infty)|^2 \lesssim r_k$, and notably the growth of the eccentricity upon exiting the resonant transition,

$$e_{\rm fin} \simeq e_{\rm cr}\sqrt{1 - {\rm e}^{-{\rm C_k}}}, \quad \text{with} \quad {\rm C_k} \sim \frac{\sqrt{\gamma_k}}{\Omega_k} b_k. \quad (18)$$

Although we have used a small-eccentricity approximation to describe the initial stages of the cloud's evolution in (6), we have demonstrated through numerical studies that the behavior described above remains valid for generic (planar) orbits. See Ref. [46] and Supplemental Material [57] for details.

The cloud's eccentric fossil—As it was argued in the literature [15–17], the distribution of masses and eccentricities observed with LISA can in principle distinguish between formation channels. However, the contrast between vacuum evolution and the large eccentricities produced by the cloud's resonant transition can lead to dramatic changes in the expected evolution of the system. As a proof of concept, we take the stellar-mass BBH population studied in [15], with chirp masses $\mathcal{M} \lesssim 10 M_\odot$, expected to form exclusively in isolation, and with the spins aligned with the orbital angular momentum. As a consequence, the assumption of equatorial (uninclined) motion may be implemented without loss of generality (as done in [15]).

We consider clouds of ultralight bosons of mass between 10^{-13} and 10^{-11} eV, surrounding black holes in co-rotating orbits. Superradiance may then excite the $|322\rangle$ state which, depending on the parent black hole's mass and birth orbital frequency, will experience a series of (hyper)fine transitions [84].

To illustrate the distinct physical effects, and following [14,15], we consider a birth orbital frequency (for the cloud + BBH system) at $\Omega_{\rm ini}/\pi \simeq 10^{-4}$ Hz [85], and evolve, using the peak GW frequency [87]

$$f_{\rm GW} \simeq \frac{\Omega}{\pi}\frac{(1+e)^{1.1954}}{(1-e^2)^{3/2}}, \quad (19)$$

until $f_{\rm GW} = 10^{-2}$ and 1 Hz. The final distribution is shown on the left panel of Fig. 1. While some of the BBHs experience an early overtone of the hyperfine transition, the majority are affected by the fine overtones instead. The BBHs then float over a period of time while increasing the orbital eccentricity. Moreover, the cloud typically either terminates there or decays later at the $k = 0$ resonance. Depending on the parameters, the ultimate decay may decrease the eccentricity or have a small impact on the orbit. As a result, a *wedge-type* distribution emerges, with

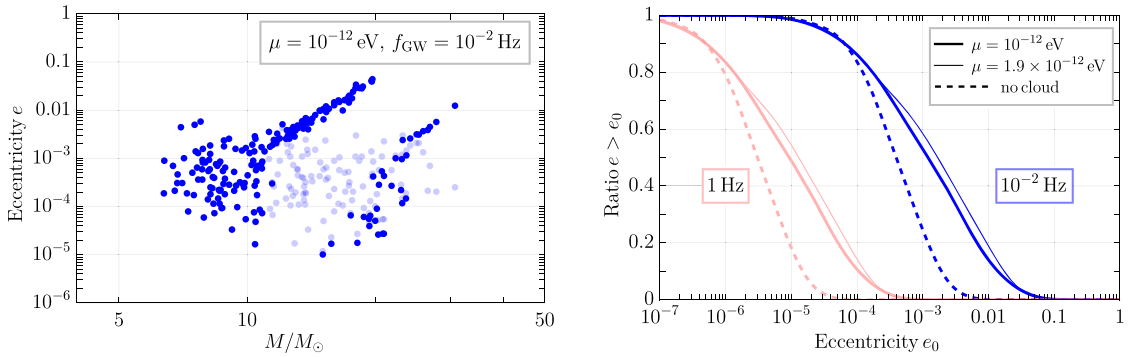

FIG. 1. BBH eccentricities at $f_{\rm GW} = 10^{-2}$ Hz (left), evolved with a uniformly distributed $q \in [0.1, 1]$ and a boson cloud on the heavier black hole. The pale blue dots account for the values without a cloud [15]. (BBHs with $e \lesssim 10^{-6}$ are not shown.) Cumulative effect, i.e., the ratio of binaries with eccentricities above a given value e_0, (right), with (solid) and without (dotted) a cloud, both at 10^{-2} Hz (blue) and 1 Hz (pink), respectively.

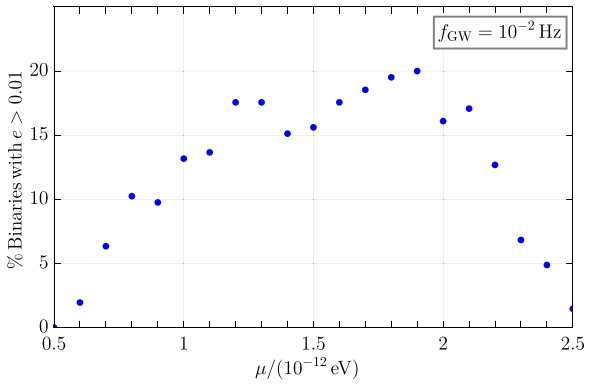

FIG. 2. Percentage of binaries with eccentricities above 0.01 at $f_{\rm GW} = 10^{-2}$ Hz for different values of μ.

the heavier black holes (within each wedge) subject to the largest increase in eccentricities.

The cumulative effect is shown on the right panel of Fig. 1, where a significant fraction of the population (with different parent masses) is affected by the resonances, yielding values of the eccentricities at 1 Hz that may be within reach of midband and decihertz detectors. As the value of μ increases (decreases) the location of the wedge in the distribution moves toward lower (higher) masses. The dependence on the value of μ for this population of BBH (with $\mathcal{M} \lesssim 10M_\odot$), reaching $e \gtrsim 10^{-2}$ at $f_{\rm GW} = 10^{-2}$ Hz, is shown in Fig. 2.

Eccentric in band—Because of the connection to formation channels, we discussed a subpopulation of BBHs. However, similar conclusions apply to black holes with higher masses [46]. For instance, for a GW170809-type event [88] ($\mathcal{M} \simeq 24M_\odot$), with a parent black hole $M \simeq 20M_\odot$ (carrying the cloud) and a (heavier) companion $M_\star \simeq 40M_\odot$, we find $f_{\rm GW} \gtrsim 10^{-2}$ Hz at the $k = -1$ fine transition for $\mu \simeq 1.5 \times 10^{-12}$ eV. The BBH reaches the resonance and floats, with approximately constant orbital frequency for about six years, while the eccentricity

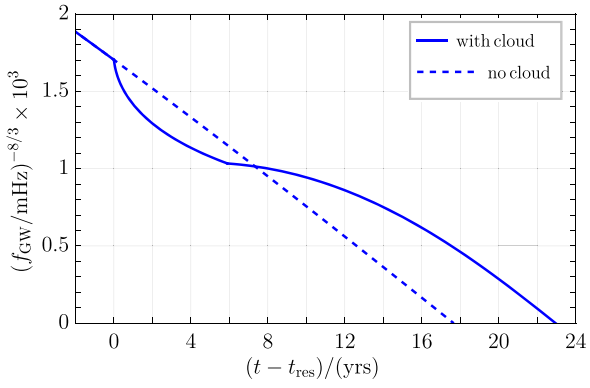

FIG. 3. Evolution of the peak frequency through a resonant transition (at $t - t_{\rm res} = 0$) in the LISA band of a GW170809-like event, compared to the evolution without the cloud.

increases from $e \lesssim 10^{-2}$ to $e \simeq 0.1$, and likewise the peak GW frequency grows, while the cloud depletes. The resulting frequency evolution till merger, which is distinct from the growth of the eccentricity that may occur due to other astrophysical mechanisms [89–91], is displayed in Fig. 3. In addition to the notable features, higher harmonics would also become more relevant as the eccentricity increases [92]. As for the case of large tidal Love numbers [37,42,93], new dedicated templates will be needed to search for these phenomena in the GW data.

Conclusions—We have shown that the presence of a boson cloud surrounding a black hole in a binary system can impact the distribution of masses and eccentricities observable with GW detectors. We have also found that a greater-than-expected value of the eccentricity, $e \gtrsim 10^{-2}$ at GW frequencies $f_{\rm GW} \simeq 10^{-2}$ Hz, develops for a (sub-)population of isolated stellar-mass BBHs (with $\mathcal{M} \lesssim 10M_\odot$), right at the heart of the LISA band. Likewise, these BBHs will decay through GW emission to values of the eccentricities, i.e., $e \simeq 10^{-4}$–10^{-3}, within experimental reach of midband [6] and decihertz [7] detectors. The observation of such GW signals would then provide tantalizing evidence for the existence of an ultralight particle of mass between 5×10^{-13} and 2.5×10^{-12} eV in nature. Furthermore, we have also shown that in-band resonance transitions are possible, yielding dramatic changes in the GW frequency evolution, constituting yet another smoking-gun signature of the imprint of a boson cloud in the BBH dynamics.

There are several venues for further exploration. First, unlike Bohr-type resonances, we have concentrated here on (corotating) hyperfine and fine transitions which occur outside of the cloud (for the range of parameters we considered), and therefore are not subject to ionization or dynamical friction [39,41]. Preliminary studies suggest that a similar increase of eccentricity occurs for certain type of Bohr transitions at higher frequencies, which would put them within reach of the ET and CE detectors [46], but a more in-depth study is needed to take all relevant effects into account. Second, although generic, we have considered the case of uninclined orbits. This is justified for the populations of BBHs we considered here (formed in isolation with spins parallel with the angular momentum). However, to encompass also dynamically formed systems, we must add inclination and new (off-plane) transitions [41]. While our results remain unchanged for quasiplanar motion, we also expect similar conclusions to apply for inclined orbits. (In fact, as shown in [95,96], resonant transitions tend to equatorialize the orbit.) Finally, identical results can be drawn also for neutron star–black hole binaries. For instance, those formed in isolation have a parent black hole with mass near $M \simeq 7M_\odot$, and likewise in binaries with negligible eccentricity at $f_{\rm GW} \simeq 1$ Hz [13,25,31]. The presence of a boson cloud would then also lead to larger-than-expected eccentricities, providing additional circumstantial evidence for a new ultralight particle in nature.

Acknowledgments—We thank G. M. Tomaselli for informative discussions and the authors of [95] for sharing a draft of their related work. The work of M. B. and M. K. is supported in part by the Deutsche Forschungsgemeinschaft (DFG, German Research Foundation) under Germany's Excellence Strategy—EXC 2121 "Quantum Universe"—390833306. M. B. and R. A. P. are supported in part by the ERC Consolidator Grant "Precision Gravity: From the LHC to LISA" provided by the European Research Council (ERC) under the European Union's H2020 research and innovation programme (Grant No. 817791).

[1] R. Abbott *et al.* (KAGRA, VIRGO, and LIGO Scientific Collaborations), Open data from the third observing run of LIGO, Virgo, KAGRA, and GEO, Astrophys. J. Suppl. Ser. **267**, 29 (2023).
[2] R. Alves Batista *et al.*, EuCAPT white paper: Opportunities and challenges for theoretical astroparticle physics in the next decade, arXiv:2110.10074.
[3] K. G. Arun *et al.* (LISA Collaboration), New horizons for fundamental physics with LISA, Living Rev. Relativity **25**, 4 (2022).
[4] M. Maggiore *et al.*, Science case for the Einstein telescope, J. Cosmol. Astropart. Phys. 03 (2020) 050.
[5] D. Reitze *et al.*, Cosmic explorer: The U.S. contribution to gravitational-wave astronomy beyond LIGO, Bull. Am. Astron. Soc. **51**, 035 (2019), https://baas.aas.org/pub/2020n7i035/release/1.
[6] S. Baum, Z. Bogorad, and P. W. Graham, Gravitational wave science in the mid-band with atom interferometers, J. Cosmol. Astropart. Phys. 05 (2024) 027.
[7] S. Kawamura *et al.*, Current status of space gravitational wave antenna DECIGO and B-DECIGO, Prog. Theor. Exp. Phys. **2021**, 05A105 (2021).
[8] A. Arvanitaki, S. Dimopoulos, S. Dubovsky, N. Kaloper, and J. March-Russell, String axiverse, Phys. Rev. D **81**, 123530 (2010).
[9] A. Arvanitaki and S. Dubovsky, Exploring the string axiverse with precision black hole physics, Phys. Rev. D **83**, 044026 (2011).
[10] D. J. E. Marsh, Axion cosmology, Phys. Rep. **643**, 1 (2016).
[11] M. Demirtas, C. Long, L. McAllister, and M. Stillman, The Kreuzer-Skarke axiverse, J. High Energy Phys. 04 (2020) 138.
[12] V. M. Mehta, M. Demirtas, C. Long, D. J. E. Marsh, L. McAllister, and M. J. Stott, Superradiance in string theory, J. Cosmol. Astropart. Phys. 07 (2021) 033.
[13] K. Belczynski, V. Kalogera, and T. Bulik, A comprehensive study of binary compact objects as gravitational wave sources: Evolutionary channels, rates, and physical properties, Astrophys. J. **572**, 407 (2001).
[14] I. Kowalska, T. Bulik, K. Belczynski, M. Dominik, and D. Gondek-Rosinska, The eccentricity distribution of compact binaries, Astron. Astrophys. **527**, A70 (2011).
[15] K. Breivik, C. L. Rodriguez, S. L. Larson, V. Kalogera, and F. A. Rasio, Distinguishing between formation channels for binary black holes with LISA, Astrophys. J. Lett. **830**, L18 (2016).
[16] A. Nishizawa, E. Berti, A. Klein, and A. Sesana, eLISA eccentricity measurements as tracers of binary black hole formation, Phys. Rev. D **94**, 064020 (2016).
[17] A. Nishizawa, A. Sesana, E. Berti, and A. Klein, Constraining stellar binary black hole formation scenarios with eLISA eccentricity measurements, Mon. Not. R. Astron. Soc. **465**, 4375 (2017).
[18] C. L. Rodriguez, M. Zevin, C. Pankow, V. Kalogera, and F. A. Rasio, Illuminating black hole binary formation channels with spins in Advanced LIGO, Astrophys. J. Lett. **832**, L2 (2016).
[19] C. L. Rodriguez, P. Amaro-Seoane, S. Chatterjee, and F. A. Rasio, Post-Newtonian dynamics in dense star clusters: Highly eccentric, highly spinning, and repeated binary black hole mergers, Phys. Rev. Lett. **120**, 151101 (2018).
[20] C. L. Rodriguez, P. Amaro-Seoane, S. Chatterjee, K. Kremer, F. A. Rasio, J. Samsing, C. S. Ye, and M. Zevin, Post-Newtonian dynamics in dense star clusters: Formation, masses, and merger rates of highly-eccentric black hole binaries, Phys. Rev. D **98**, 123005 (2018).
[21] M. E. Lower, E. Thrane, P. D. Lasky, and R. Smith, Measuring eccentricity in binary black hole inspirals with gravitational waves, Phys. Rev. D **98**, 083028 (2018).
[22] L. Randall and Z.-Z. Xianyu, Eccentricity without measuring eccentricity: Discriminating among stellar mass black hole binary formation channels, Astrophys. J. **914**, 75 (2021).
[23] X. Fang, T. A. Thompson, and C. M. Hirata, The population of eccentric binary black holes: Implications for mHz gravitational wave experiments, Astrophys. J. **875**, 75 (2019).
[24] I. M. Romero-Shaw, P. D. Lasky, E. Thrane, and J. C. Bustillo, GW190521: Orbital eccentricity and signatures of dynamical formation in a binary black hole merger signal, Astrophys. J. Lett. **903**, L5 (2020).
[25] M. A. Sedda, Dissecting the properties of neutron star–black hole mergers originating in dense star clusters, Commun. Phys. **3**, 43 (2020).
[26] H. Glanz and H. B. Perets, Common envelope evolution of eccentric binaries, Mon. Not. R. Astron. Soc. **507**, 2659 (2021).
[27] M. Zevin, I. M. Romero-Shaw, K. Kremer, E. Thrane, and P. D. Lasky, Implications of eccentric observations on binary black hole formation channels, Astrophys. J. Lett. **921**, L43 (2021).
[28] A. Gualandris, F. M. Khan, E. Bortolas, M. Bonetti, A. Sesana, P. Berczik, and K. Holley-Bockelmann, Eccentricity evolution of massive black hole binaries from formation to coalescence, Mon. Not. R. Astron. Soc. **511**, 4753 (2022).
[29] M. Garg, S. Tiwari, A. Derdzinski, J. G. Baker, S. Marsat, and L. Mayer, The minimum measurable eccentricity from gravitational waves of LISA massive black hole binaries, Mon. Not. R. Astron. Soc. **528**, 4176 (2024).
[30] P. Saini, Resolving the eccentricity of stellar mass binary black holes with next generation ground-based gravitational wave detectors, Mon. Not. R. Astron. Soc. **528**, 833 (2024).
[31] R. Dhurkunde and A. H. Nitz, Search for eccentric NSBH and BNS mergers in the third observing run of Advanced LIGO and Virgo, arXiv:2311.00242.

[32] Y. B. Zel'Dovich, Generation of waves by a rotating body, JETP Lett. **14**, 180 (1971), https://ui.adsabs.harvard.edu/abs/1971JETPL..14..180Z/abstract.
[33] Y. B. Zel'Dovich, Amplification of cylindrical electromagnetic waves reflected from a rotating body, Sov. J. Exp. Theor. Phys. **35**, 1085 (1972), https://ui.adsabs.harvard.edu/abs/1972JETP...35.1085Z/abstract.
[34] W. H. Press and S. A. Teukolsky, Floating orbits, superradiant scattering and the black-hole bomb, Nature (London) **238**, 211 (1972).
[35] W. E. East, Massive boson superradiant instability of black holes: Nonlinear growth, saturation, and gravitational radiation, Phys. Rev. Lett. **121**, 131104 (2018).
[36] R. Brito, V. Cardoso, and P. Pani, Superradiance: New frontiers in black hole physics, Lect. Notes Phys. **906**, 1 (2015).
[37] D. Baumann, H. S. Chia, and R. A. Porto, Probing ultralight bosons with binary black holes, Phys. Rev. D **99**, 044001 (2019).
[38] D. Baumann, H. S. Chia, R. A. Porto, and J. Stout, Gravitational collider physics, Phys. Rev. D **101**, 083019 (2020).
[39] D. Baumann, G. Bertone, J. Stout, and G. M. Tomaselli, Ionization of gravitational atoms, Phys. Rev. D **105**, 115036 (2022).
[40] D. Baumann, G. Bertone, J. Stout, and G. M. Tomaselli, Sharp signals of boson clouds in black hole binary inspirals, Phys. Rev. Lett. **128**, 221102 (2022).
[41] G. M. Tomaselli, T. F. M. Spieksma, and G. Bertone, Dynamical friction in gravitational atoms, J. Cosmol. Astropart. Phys. 07 (2023) 070.
[42] H. S. Chia, T. D. P. Edwards, D. Wadekar, A. Zimmerman, S. Olsen, J. Roulet, T. Venumadhav, B. Zackay, and M. Zaldarriaga, In pursuit of Love: First templated search for compact objects with large tidal deformabilities in the LIGO-Virgo Data, arXiv:2306.00050.
[43] P. C. Peters and J. Mathews, Gravitational radiation from point masses in a Keplerian orbit, Phys. Rev. **131**, 435 (1963).
[44] P. C. Peters, Gravitational radiation and the motion of two point masses, Phys. Rev. **136**, B1224 (1964).
[45] E. Berti, R. Brito, C. F. B. Macedo, G. Raposo, and J. L. Rosa, Ultralight boson cloud depletion in binary systems, Phys. Rev. D **99**, 104039 (2019).
[46] M. Boskovic, M. Koschnitzke, and R. A. Porto (to be published).
[47] S. L. Detweiler, Klein-Gordon equation and rotating black holes, Phys. Rev. D **22**, 2323 (1980).
[48] D. Baumann, H. S. Chia, J. Stout, and L. ter Haar, The spectra of gravitational atoms, J. Cosmol. Astropart. Phys. 12 (2019) 006.
[49] W. E. East, Superradiant instability of massive vector fields around spinning black holes in the relativistic regime, Phys. Rev. D **96**, 024004 (2017).
[50] S. R. Dolan, Instability of the massive Klein-Gordon field on the Kerr spacetime, Phys. Rev. D **76**, 084001 (2007).
[51] H. Yoshino and H. Kodama, Gravitational radiation from an axion cloud around a black hole: Superradiant phase, Prog. Theor. Exp. Phys. **2014**, 043E02 (2014).
[52] R. Brito, V. Cardoso, and P. Pani, Black holes as particle detectors: Evolution of superradiant instabilities, Classical Quantum Gravity **32**, 134001 (2015).
[53] A. Arvanitaki, M. Baryakhtar, and X. Huang, Discovering the QCD axion with black holes and gravitational waves, Phys. Rev. D **91**, 084011 (2015).
[54] R. Brito, S. Ghosh, E. Barausse, E. Berti, V. Cardoso, I. Dvorkin, A. Klein, and P. Pani, Gravitational wave searches for ultralight bosons with LIGO and LISA, Phys. Rev. D **96**, 064050 (2017).
[55] N. Siemonsen, T. May, and W. E. East, Modeling the black hole superradiance gravitational waveform, Phys. Rev. D **107**, 104003 (2023).
[56] This approximation turns out to be extremely accurate, upon comparison with numerical solutions for generic (planar) orbits, for most of the parameter space. (See Supplemental Material [57].)
[57] See Supplemental Material at http://link.aps.org/supplemental/10.1103/PhysRevLett.133.121401 for further details, which includes [58–71].
[58] H. Yoshino and H. Kodama, The bosenova and axiverse, Classical Quantum Gravity **32**, 214001 (2015).
[59] A. Gruzinov, Black hole spindown by light bosons, arXiv:1604.06422.
[60] M. Baryakhtar, M. Galanis, R. Lasenby, and O. Simon, Black hole superradiance of self-interacting scalar fields, Phys. Rev. D **103**, 095019 (2021).
[61] H. S. Chia, C. Doorman, A. Wernersson, T. Hinderer, and S. Nissanke, Self-interacting gravitational atoms in the strong-gravity regime, J. Cosmol. Astropart. Phys. 04 (2023) 018.
[62] J. a. G. Rosa and T. W. Kephart, Stimulated axion decay in superradiant clouds around primordial black holes, Phys. Rev. Lett. **120**, 231102 (2018).
[63] M. Boskovic, R. Brito, V. Cardoso, T. Ikeda, and H. Witek, Axionic instabilities and new black hole solutions, Phys. Rev. D **99**, 035006 (2019).
[64] H. Fukuda and K. Nakayama, Aspects of nonlinear effect on black hole superradiance, J. High Energy Phys. 01 (2020) 128.
[65] T. F. M. Spieksma, E. Cannizzaro, T. Ikeda, V. Cardoso, and Y. Chen, Superradiance: Axionic couplings and plasma effects, Phys. Rev. D **108**, 063013 (2023).
[66] Y. Chen, X. Xue, and V. Cardoso, Black holes as neutrino factories, arXiv:2308.00741.
[67] E. Cannizzaro, L. Sberna, S. R. Green, and S. Hollands, Relativistic perturbation theory for black-hole boson clouds, Phys. Rev. Lett. **132**, 051401 (2024).
[68] F. Duque, C. F. B. Macedo, R. Vicente, and V. Cardoso, Axion weak leaks: Extreme mass-ratio inspirals in ultralight dark matter, arXiv:2312.06767.
[69] S. L. Detweiler and E. Poisson, Low multipole contributions to the gravitational self-force, Phys. Rev. D **69**, 084019 (2004).
[70] Y. Cao and Y. Tang, Signatures of ultralight bosons in compact binary inspiral and outspiral, Phys. Rev. D **108**, 123017 (2023).
[71] W. R. Inc., Mathematica, Version 13.2, Champaign, IL, 2022, https://www.wolfram.com/mathematica.
[72] S. Tremaine, *Dynamics of Planetary Systems* (Princeton University Press, Princeton, New Jersey, 2023).

[73] L. Landau, Zur theorie der energieubertragung. II (1932), https://cir.nii.ac.jp/crid/1370290617742844819.
[74] C. Zener, Nonadiabatic crossing of energy levels, Proc. R. Soc. A **137**, 696 (1932).
[75] V. M. Akulin and W. P. Schleich, Landau-Zener transition to a decaying level, Phys. Rev. A **46**, 4110 (1992).
[76] R. Brito and S. Shah, Extreme mass-ratio inspirals into black holes surrounded by scalar clouds, Phys. Rev. D **108**, 084019 (2023).
[77] N. V. Vitanov and S. Stenholm, Pulsed excitation of a transition to a decaying level, Phys. Rev. A **55**, 2982 (1997).
[78] T. Takahashi, H. Omiya, and T. Tanaka, Evolution of binary systems accompanying axion clouds in extreme mass ratio inspirals, Phys. Rev. D **107**, 103020 (2023).
[79] T. Takahashi, H. Omiya, and T. Tanaka, Axion cloud evaporation during inspiral of black hole binaries: The effects of backreaction and radiation, Prog. Theor. Exp. Phys. **2022**, 043E01 (2022).
[80] G. Ficarra, P. Pani, and H. Witek, Impact of multiple modes on the black-hole superradiant instability, Phys. Rev. D **99**, 104019 (2019).
[81] L. Hui, Y. T. A. Law, L. Santoni, G. Sun, G. M. Tomaselli, and E. Trincherini, Black hole superradiance with dark matter accretion, Phys. Rev. D **107**, 104018 (2023).
[82] We ignore here effects due to changes in the background (M, S) black hole's parameters. We justify this approximation in Supplemental Material [57], see also [46].
[83] N. V. Vitanov, Transition times in the Landau-Zener model, Phys. Rev. A **59**, 988 (1999).
[84] For the BBH population and values of μ we consider here, the largest impact on the orbital evolution happens for $\alpha \gtrsim 0.1$. Hence, the overall effect from the earlier, but shorter-lived, $|211\rangle$ component of the cloud becomes subdominant.
[85] Even in cases where the birth orbital frequency of the binary system may be lower, stellar evolution [86] can also lead to younger (secondary) black holes carrying the cloud.
[86] K. Belczynski *et al.*, Evolutionary roads leading to low effective spins, high black hole masses, and O1/O2 rates for LIGO/Virgo binary black holes, Astron. Astrophys. **636**, A104 (2020).
[87] L. Wen, On the eccentricity distribution of coalescing black hole binaries driven by the Kozai mechanism in globular clusters, Astrophys. J. **598**, 419 (2003).
[88] B. P. Abbott *et al.* (LIGO Scientific and Virgo Collaborations), GWTC-1: A gravitational-wave transient catalog of compact binary mergers observed by LIGO and Virgo during the first and second observing runs, Phys. Rev. X **9**, 031040 (2019).
[89] L. Randall and Z.-Z. Xianyu, An analytical portrait of binary mergers in hierarchical triple systems, Astrophys. J. **864**, 134 (2018).
[90] L. Randall and Z.-Z. Xianyu, Observing eccentricity oscillations of binary black holes in LISA, arXiv:1902.08604.
[91] For instance, compare the oscillatory behavior due to the presence of a third body shown in Fig. 1 of [90], with the effect of a resonant transition displayed in Fig. 3.
[92] D. Wadekar, J. Roulet, T. Venumadhav, A. K. Mehta, B. Zackay, J. Mushkin, S. Olsen, and M. Zaldarriaga, New black hole mergers in the LIGO-Virgo O3 data from a gravitational wave search including higher-order harmonics, arXiv:2312.06631.
[93] A fraction of the cloud may still survive the resonant floating period(s), even for large decaying widths, which can also produce a measurable imprint in the waveforms through finite-size effects [37] (see also [94]).
[94] B. Su, Z.-Z. Xianyu, and X. Zhang, Probing ultralight bosons with compact eccentric binaries, Astrophys. J. **923**, 114 (2021).
[95] G. M. Tomaselli, T. F. M. Spieksma, and G. Bertone, companion paper, Resonant history of gravitational atoms in black hole binaries, Phys. Rev. D **110**, 064048 (2024).
[96] G. M. Tomaselli, T. F. M. Spieksma, and G. Bertone, following Letter, Legacy of boson clouds on black hole binaries, Phys. Rev. Lett. **133**, 121402 (2024).